High-density electroencephalographic functional networks in genetic generalized epilepsy: Preserved whole-brain topology hides local reorganization

André Silva Alves, Isotta Rigoni, Pierre Mégevand, Stanislas Lagarde, Fabienne Picard, Margitta Seeck, Serge Vulliémoz, Nicolas Roehri

Received: 4 September 2023 | Revised: 15 January 2024 | Accepted: 16 January 2024

DOI: 10.1111/epi.17903

Epilepsia®

RESEARCH ARTICLE

High-density electroencephalographic functional networks in genetic generalized epilepsy: Preserved whole-brain topology hides local reorganization

André Silva Alves[1] | Isotta Rigoni[1] | Pierre Mégevand[1] | Stanislas Lagarde[1,2] | Fabienne Picard[1] | Margitta Seeck[1] | Serge Vulliémoz[1] | Nicolas Roehri[1]

[1]EEG and Epilepsy Unit, University Hospitals and Faculty of Medicine, University of Geneva, Geneva, Switzerland

[2]Aix Marseille University, Inserm, INS, Institut de Neurosciences des Systèmes, Marseille, France

Correspondence
Nicolas Roehri, EEG and Epilepsy Unit, University Hospitals and Faculty of Medicine, University of Geneva, Rue Gabrielle-Perret-Gentil 4, 1205 Geneva, Switzerland.
Email: nicolas.roehri@unige.ch

Funding information
Schweizerischer Nationalfonds zur Förderung der Wissenschaftlichen Forschung, Grant/Award Number: 170873, 180365, 192749, 194507, 209120 and 209470

Abstract

Objective: Genetic generalized epilepsy (GGE) accounts for approximately 20% of adult epilepsy cases and is considered a disorder of large brain networks, involving both hemispheres. Most studies have not shown any difference in functional whole-brain network topology when compared to healthy controls. Our objective was to examine whether this preserved global network topology could hide local reorganizations that balance out at the global network level.

Methods: We recorded high-density electroencephalograms from 20 patients and 20 controls, and reconstructed the activity of 118 regions. We computed functional connectivity in windows free of interictal epileptiform discharges in broad, delta, theta, alpha, and beta frequency bands, characterized the network topology, and used the Hub Disruption Index (HDI) to quantify the topological reorganization. We examined the generalizability of our results by reproducing a 25-electrode clinical system.

Results: Our study did not reveal any significant change in whole-brain network topology among GGE patients. However, the HDI was significantly different between patients and controls in all frequency bands except alpha ($p < .01$, false discovery rate [FDR] corrected, $d < -1$), and accompanied by an increase in connectivity in the prefrontal regions and default mode network. This reorganization suggests that regions that are important in transferring the information in controls were less so in patients. Inversely, the crucial regions in patients are less so in controls. These findings were also found in delta and theta frequency bands when using 25 electrodes ($p < .001$, FDR corrected, $d < -1$).

Significance: In GGE patients, the overall network topology is similar to that of healthy controls but presents a balanced local topological reorganization. This reorganization causes the prefrontal areas and default mode network to be more integrated and segregated, which may explain executive impairment associated with GGE. Additionally, the reorganization distinguishes patients from controls even when using 25 electrodes, suggesting its potential use as a diagnostic tool.

KEYWORDS
clustering coefficient, electrical source imaging, global efficiency, hdEEG, homeostasis

1 | INTRODUCTION

Genetic generalized epilepsy (GGE) encompasses a group of syndromes with high heritability and complex polygenic inheritance, characterized by widespread bilateral cortical hyperexcitability that results in various types of seizures, such as myoclonic, absence, or generalized tonic–clonic seizures.[1] In adults, GGE accounts for approximately 20% of all epilepsy cases.[2] Unlike focal epilepsies, GGE is typically characterized by widespread atypical cortical activity, including generalized (poly)spike-and-wave discharges (GSW), rather than abnormal brain anatomy or focal electroencephalographic (EEG) abnormalities. Unfortunately, in a minority of GGE patients, interictal GSW may be scarce or absent, causing diagnostic delays with severe consequences. Identifying EEG markers of GGE beyond GSW occurrence could be a valuable clinical tool. EEG–functional magnetic resonance imaging (fMRI) and magnetoencephalography (MEG) studies have demonstrated the involvement of the thalamus and a large frontoparietal network during GSW.[3–5] These regions overlap with the default mode network (DMN), one of the intrinsic patterns of spontaneous cerebral activity, mostly active during rest.[6] Additionally, volumetric and microstructural alterations have been identified in similar regions using different MRI techniques when comparing patients to healthy controls.[7–9] These findings provide evidence for a restricted network involvement in GGE rather than a whole-brain disease.

In focal epilepsy, increased functional connectivity has often been related to the epileptogenic zone.[10–12] In patients with GGE, there is a general increase in functional connectivity.[13] One would therefore expect a global impact on the functional structure and efficiency of the brain, that is, on its network topology. A recent review and meta-analysis found no evidence supporting this hypothesis, showing similar brain network topology in GGE patients and healthy controls for fMRI, EEG, and MEG.[14,15] Achard et al.[16] encountered a similar paradox with comatose patients, who exhibited a network topology similar to that of healthy subjects. To quantify local topological network reorganization, they designed the Hub Disruption Index (HDI). Their findings revealed that the regions crucial in transferring neural information across the network in healthy participants were less important in patients. Conversely, less central regions in controls became more crucial in patients, resulting in an equivalent overall network topology. We hypothesized that whole-brain network topology would be similar in GGE patients and healthy controls, but that this preserved topology would be the result of a balanced reorganization across regions. We postulated that the frontal networks and DMN, key networks in GGE, would be involved in the reorganization.

Key points

- The brain topology of patients with GGE is similar to that of healthy controls
- Local topological reorganizations, quantified by the HDI, occur in GGE but balance out at the global network level
- The increase of topological features occurs in frontal areas and default mode network and is accompanied by an increase in connectivity
- The HDI separates GGE patients from healthy controls, even in a 25-electrode setting, suggesting its use as a diagnostic tool
- The HDI was not correlated with the rate of epileptiform discharges or drug load

In this study, we aimed to investigate brain network topology of patients with GGE using high-density EEG. We performed a connectivity analysis in source-space, utilizing regions of interest, to identify differences in network topology in GGE patients. We aimed to identify the topography of these network reorganizations in different frequency bands using the HDI, and quantify how well this measure separates patients from controls. To assess the generalizability and diagnostic potential of our findings, we conducted the same analysis using a 25-electrode EEG montage.

2 | MATERIALS AND METHODS

2.1 | Participants

For this study, we recruited patients with GGE and healthy controls. Based on retrospective and prospective data from the high-density EEG (hdEEG) database of the Geneva University Hospital, we included participants according to the following criteria: >18 years old, without previous neurosurgical operation, no contraindication for MRI, and any multifocal epileptic disorder. To ensure that the patient and control groups were sex and age balanced,

we computed Fisher exact test and Wilcoxon rank sum test for the sex and age, respectively. The study was approved by the Geneva ethical committee (protocol #2020-02526). This research project was conducted in accordance with Swiss regulations and with the Declaration of Helsinki.

2.2 | EEG processing

All participants were asked to stay calm and keep their eyes closed without sleeping during an hdEEG recording (256 electrodes, Electrical Geodesic system, sampling rate of 1000 Hz). Patients and controls were recorded in the same setting; controls were recorded for 10 min and patients for 20 min to account for epochs removed due to the presence of interictal epileptiform discharges (IEDs). The EEG recordings were downsampled to 250 Hz and filtered using a zero-phase distortion digital 4th-order Butterworth bandpass filter between 1 and 45 Hz. In addition, a 50-Hz notch filter was applied to suppress the power line noise. Infomax-based independent component analysis was applied to remove oculomotor, cardiac, and muscle artifacts following the recommendations by Jung et al.[17] Bad electrodes were interpolated using a three-dimensional spherical spline,[18] and electrodes from the cheeks and the neck were removed from further analysis, as their signal is generally contaminated by artifact,[19] leaving 204 electrodes. Finally, the data were rereferenced to the common average reference. The EEG preprocessing stages were performed using Fieldtrip Toolbox.[20] IEDs were marked by an expert epileptologist (S.L.); the number of marked IEDs and their rate is reported in Table S1.

2.3 | MRI processing and electrical source imaging

Individual structural T1-weighted MRI (3 T, Siemens Prisma) was available for each participant. We parceled the gray matter into 128 regions of interest (ROIs) based on the second scale of the Lausanne atlas (version 2018)[21,22] using FreeSurfer v7.0.1[23] and Connectome Mapper (v3.0.0-beta-RC1) open-source preprocessing software.[24,25] Subcortical structures such as thalamus, caudate, putamen, pallidum, and nucleus accumbens were removed from the ROIs; 118 ROIs were retained for the analyses. For the electrical source imaging (ESI), approximately 5000 sources with unconstrained orientation were equally distributed within the gray matter volume. The EEG forward model was computed with the boundary element method for a three-layer model using OpenMEEG[26] and default conductivity values. eLORETA was then used for the inverse solution.[27] The ESI was obtained using Fieldtrip Toolbox.[20] Source time series were summarized at each ROI by using singular-value decomposition of all sources within the same ROI,[28] depicted in Figure 1A.

2.4 | ROI-to-ROI connectivity

Functional connectivity was assessed using the debiased weighted phase lag index (wPLI),[29] a measure that determines the level of phase-synchrony between any given pair of ROIs and is robust to source leakage. wPLI was computed between 1 and 40 Hz, using 5-s sliding time windows with 50% overlap, and averaged for each frequency band (broad: 1–40 Hz, δ: 1–4 Hz, θ: 4–8 Hz, α: 8–12 Hz, β: 12–30 Hz). Windows containing IEDs or artifacts were rejected before computing the wPLI. To mitigate the effect of rejected windows across participants and groups, we randomly selected a maximum of 200 windows. For each participant and each frequency band, the matrices were normalized by dividing each value by the sum of all connectivity values, which is recommended to compute the clustering coefficient.[30] Finally, for each patient, a three-dimensional array (ROIs × ROIs × bands) was used to represent the weighted interaction between ROIs for each frequency band (Figure 1B).

2.5 | Network analysis

Brain network topology was studied at the global network level and at the ROI level, by quantifying two topological features: segregation and integration. Segregation corresponds to the ability of specialized processing to occur within densely interconnected groups of regions (modules); integration quantifies the network's ability to rapidly combine information from distributed brain regions (exemplified in Figure S1). As a measure of integration, we calculated the nodal efficiency (NE), which quantifies the average of the inverse shortest path length connecting the ROI to any other region.[31] Because we used weighted matrices, the path length is defined as the sum of the inverse of the weights along the path. By averaging this measure over all ROIs, we obtained the global efficiency (GE), its counterpart at the global network level. As a measure of segregation, we computed the clustering coefficient (CC),[32] which quantifies the prevalence of densely interconnected regions around individual regions (i.e., how, on average, a region and any two of its neighbors are strongly connected, all together).[33] Its counterpart at the network level is the average clustering coefficient (⟨CC⟩), which describes the level of segregation of the network. These measures were computed for each frequency band and each participant, as illustrated in Figure 1B.

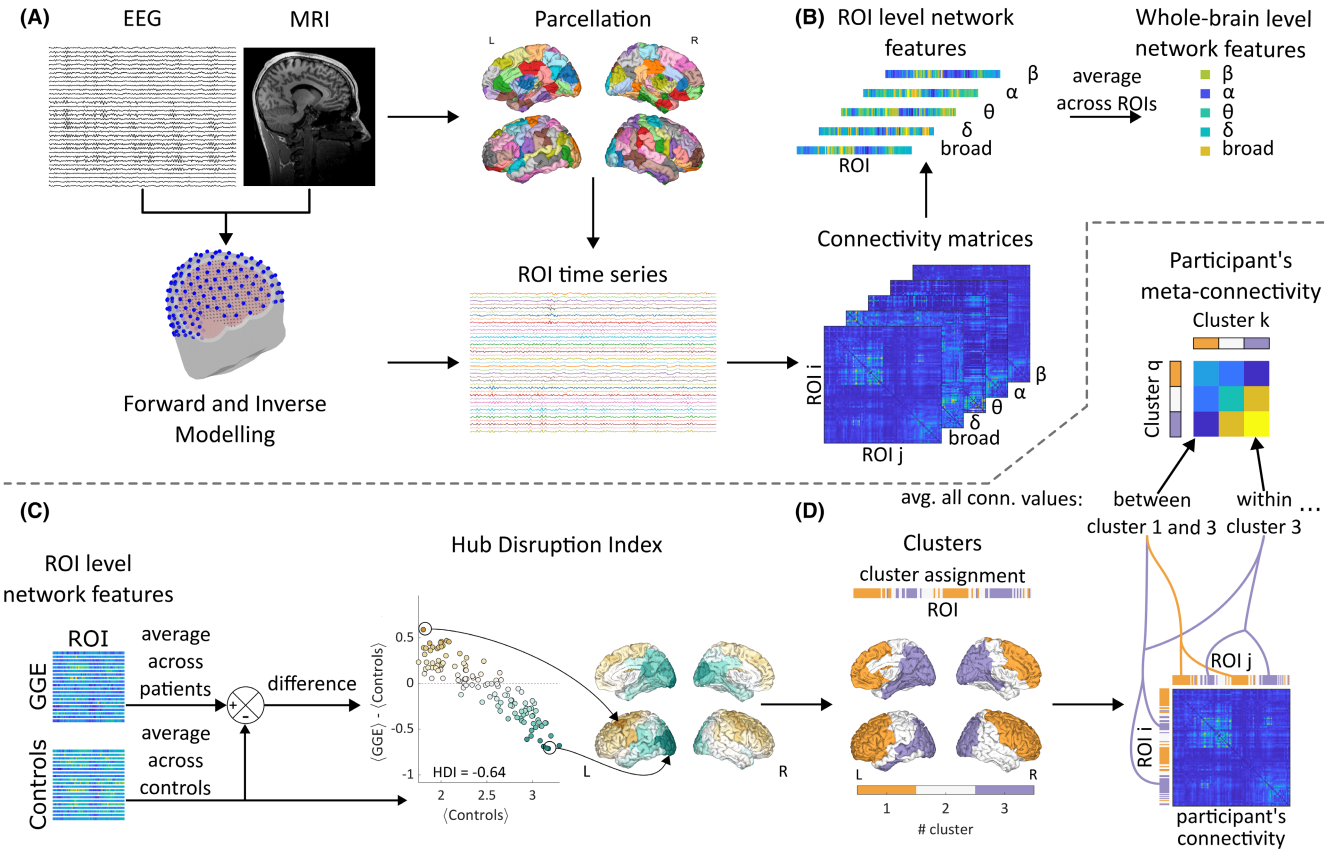

FIGURE 1 Preprocessing and analyzing pipeline, showing electroencephalographic (EEG) and magnetic resonance imaging (MRI) preprocessing (A) followed by connectivity and network analyses (B), and computation of the Hub Disruption Index (HDI) from the region of interest (ROI)-level network features (C) followed by ROI clustering to compute the participants' meta-connectivity matrix (D). (A) The individual EEG and MRI are preprocessed to obtain the forward model and inverse solution. The MRI is parcellated into 118 ROIs, onto which are projected the EEG traces to obtain the ROI time series. (B) The connectivity matrices are estimated from those time series in different frequency bands. From those matrices, we computed the ROI-level network features and averaged them to obtain their whole-brain counterparts. As network features, we investigated the integration and segregation. These measures are illustrated below (Figure S1). (C) The y-axis of the scatterplot corresponds to the difference in average ROI features between the genetic generalized epilepsy (GGE) and control groups (⟨GGE⟩-⟨Controls⟩). The x-axis corresponds to the ROI features averaged across the control group (⟨Controls⟩). One dot in the scatterplot corresponds to one ROI. The slope of the scatterplot represents the HDI. A negative slope indicates a network reorganization, namely that ROIs important in transferring information within the network of the control group are less important in that of the GGE group, and inversely. (D) Using the scatterplots of the nodal integration and segregation, we clustered the ROIs into three groups. We then computed the connectivity within and between these clusters, that is, the meta-connectivity, for each participant. For instance, the connectivity values between all ROIs assigned to the third cluster (purple) are averaged to obtain the within meta-connectivity of cluster 3. Similarly, the connectivity values between ROIs assigned to cluster 1 (orange) and those assigned to cluster 3 (purple) are averaged to obtain the meta-connectivity between cluster 1 and cluster 3. Comparing the meta-connectivity between the two groups indicates whether the network reorganization is accompanied by a change in connectivity weights. L, left; R, right.

We calculated the HDI of the functional connectivity, which assesses, at the group level, whether there is a network reorganization at the ROI level.[16] The HDI corresponds to the slope of the linear regression between the average value of a specific topological measure (NE or CC) at each ROI in the control group (x-axis) and the difference between the average value in the patient and control groups at each ROI (y-axis; Figure 1C). A negative linear relationship indicates that the ROIs with high values in the control group have lower values in patients and conversely ROIs with low values in the controls have higher values in patients. This measure will be referred to as *group HDI*. The group HDI was calculated for the NE and CC at each frequency band. Then, we calculated the *individual HDI* obtained by using the values of one participant (patient or control) versus the average of the control group. We expected the individual HDI of the controls to be approximately zero and the ones of the patients to be less than zero.[16] This individual index was calculated for the NE and CC at each frequency band and for each participant. The network features were computed using the Brain Connectivity Toolbox.[30]

2.6 | Meta-connectivity analysis

To investigate whether the changes found in NE and CC are accompanied with a change of connectivity strength, we applied the following procedure. We clustered the ROIs into three groups based on the coordinates of the ROIs in the scatterplots used to compute the HDI for both the NE and CC (Figure 1D). For each narrow frequency band showing a significant difference in individual HDIs, three clusters were obtained using a k-means clustering with the Euclidean distance and 50 replications. We then computed the meta-connectivity within and between these clusters by averaging the connectivity values of each pair of ROIs belonging to the investigated clusters, yielding a symmetric 3-by-3 meta-connectivity matrix for each patient and control, and for each frequency band (Figure 1D).

2.7 | Correlation with clinical variables

We investigated whether the individual HDIs were correlated to clinical variables (i.e., age at epilepsy onset and epilepsy duration) using the Spearman correlation. To assess potential confounding factors, we computed the Spearman correlation between the individual HDIs and the IED rates and the drug load. The drug load was calculated as the sum of the ratios between the actual dose and the defined daily dose over all antiseizure medication (ASM; Table S1).[34]

2.8 | Generalizability to standard EEG

To evaluate whether the results obtained for the group and individual HDIs were generalizable to clinical routine EEG recordings, we spatially downsampled the preprocessed EEG and reran the pipeline described above. Namely, we analyzed only the electrodes of the Electrical Geodesics, Inc. system that overlapped with the 25-channel array recommended by the International Federation of Clinical Neurophysiology.[35] This analysis aims to assess whether the individual HDIs could potentially be used as a diagnostic tool in clinical practice.

2.9 | Statistical analysis

For the network level measures (GE and ⟨CC⟩), a two-sided two-sample *t*-test with unequal variances was applied for each frequency band to the log-transformed values to compare the segregation and integration between patients and controls. This corresponded to 10 tests (i.e., two measures—GE and ⟨CC⟩—and five frequency bands) that were not corrected for multiple comparisons to demonstrate their lack of significant difference even before applying the correction for multiple comparisons. For the HDI to be meaningful, it is crucial that these measures are not statistically significant, as it quantifies the local reorganization within a preserved whole-brain network topology. This underlines our decision not to correct for multiple comparisons.

For the individual HDI, we computed a two-sided two-sample *t*-test with unequal variances to examine whether there was a significant difference between the individual HDI of patients and controls as in Achard et al.[16] These *t*-tests were controlled for 10 comparisons (two features—HDI,NE and HDI,CC—and five frequency bands) with the false discovery rate (FDR) procedure ($Q < .05$).[36] Cohen's *d* was used to quantify the effect size.

For the individual HDI computed using a standard 25-channel EEG, only previously significant frequency bands were tested (i.e., broad, delta, theta, beta bands) using the same *t*-test as above. These *t*-tests were controlled for eight comparisons (two features—HDI,NE and HDI,CC—and four frequency bands) with the FDR procedure ($Q < .05$).[36] Cohen's *d* was used to quantify the effect size.

For the meta-connectivity analysis, the values of the symmetric 3-by-3 matrices were log-transformed and compared between patients and controls using a two-sided two-sample *t*-test with unequal variances, and corrected for multiple comparisons with the FDR procedure (corrected for 18 comparisons: six edges and three frequency bands—delta, theta, beta).

3 | RESULTS

3.1 | Participants' demographics

Twenty adults with GGE (12 women, median age at the time of the EEG recording was 31.5 years, range = 18–57, median epilepsy duration was 15.5 years, range = 7–44) were recruited from the EEG and Epilepsy Unit at the University Hospital of Geneva (Table S1). Twenty controls (10 women, median age at the time of the EEG recording was 31 years, range = 23–54) were also recorded. There was no significant difference in terms of sex ($p = .53$, odds ratio = .55) and age ($p = .89$, *z*-value = .136) between the two groups.

3.2 | Global network measures

GE and ⟨CC⟩ (Figure 2) showed no significant difference ($p > .05$, uncorrected) between patients and controls in any frequency band.

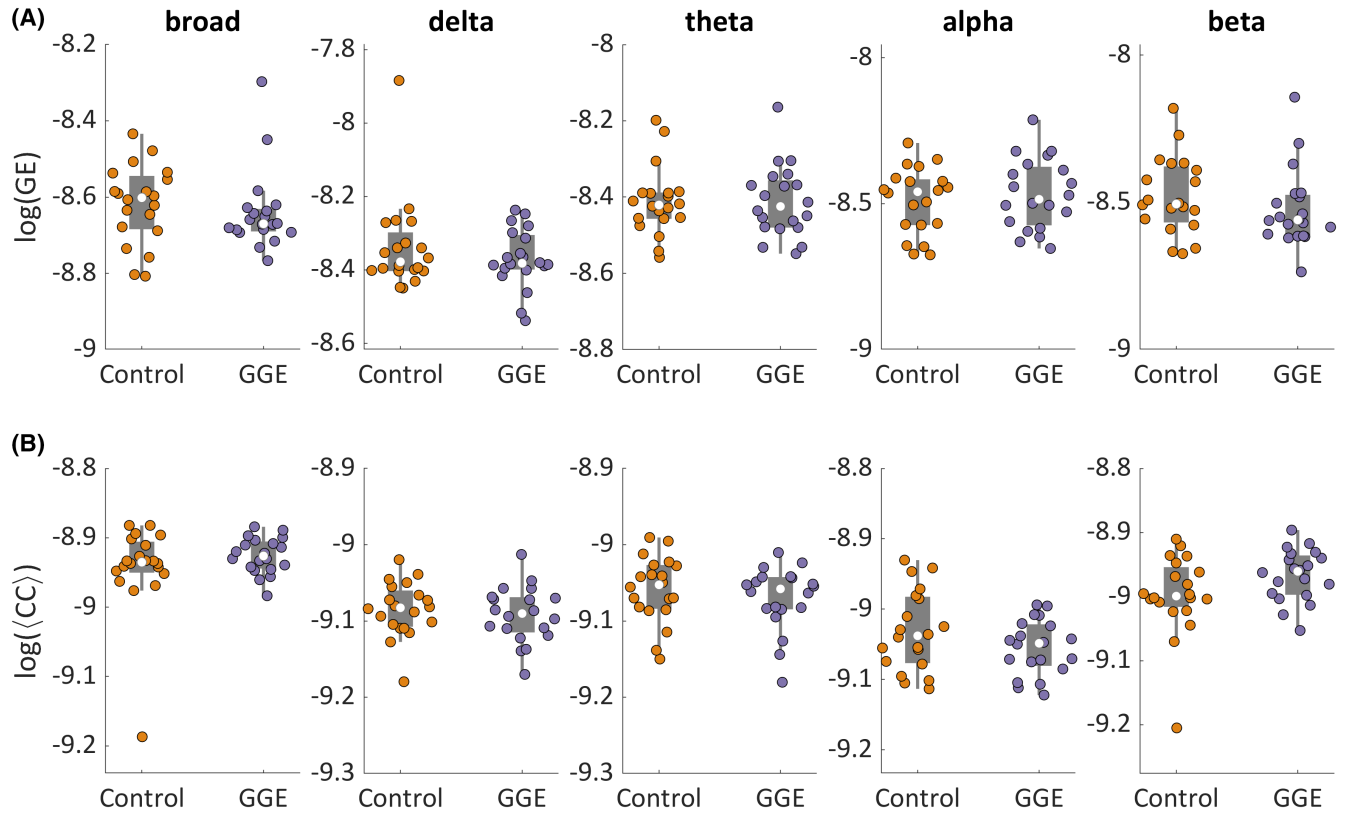

FIGURE 2 Network integration and segregation in healthy control participants and patients across five frequency bands. The swarm plot and boxplot of the integration, estimated with the global efficiency (GE), is shown in panel A for the five frequency bands. The segregation estimated with the average clustering coefficient (⟨CC⟩) is shown in panel B. All values were log-transformed to improve their normality. No significant differences in either integration or segregation were found ($p > .05$, uncorrected). GGE, genetic generalized epilepsy.

3.3 | Disruption of local network measures

The group HDIs for NE and CC were negative in all frequency bands (broad: −.64|−.58, δ: −.75|−.83, θ: −.83|−.87, α: −.22|−.34, β: −.70|−.67; Figures 3 and 4), meaning that ROIs with the higher NE or CC in controls had lower values in patients and that ROIs with lower values in controls had higher values in patients. The individual HDIs were significantly lower for NE and CC in the broad ($t = -2.64|-2.70$, $p = .016|.016$, $d = -.84|-.86$), δ ($t = -2.68|-3.64$, $p = .016|.0044$, $d = -.84|-1.15$), θ ($t = -3.48|-3.67$, $p = .0047|.0044$, $d = -1.10|-1.16$), and β ($t = -3.25|-2.93$, $p = .006|.012$, $d = -1.03|-.92$) bands in GGE compared to controls (Figures 3 and 4). In the alpha band, there was no significant differences for either measure ($t = -1.03|-1.55$, $p = .31|.14$, $d = -.32|-.49$).

Spatially, in the broad and beta bands, both network properties followed a negative anteroposterior gradient, with the ROIs of the prefrontal cortex having an increase in NE and CC compared to controls (colored brown, Figures 3–4 A and E) and ROIs of the occipital lobe having a decrease (colored green, Figures 3–4 A and E). In the delta band, it followed a negative dorsoventral gradient, with a maximum increase in the right caudal motor cortex and decrease in the left anterior middle temporal gyrus. In the theta band, the NE and CC of ROIs corresponding visually to the DMN (e.g., medial prefrontal cortex, precuneus, inferior parietal lobule) were higher in patients, whereas regions belonging to the limbic system (e.g., insula, cingulate cortex) as well as the temporal lobes were lower in patients versus controls.

3.4 | Differences in meta-connectivity

The clusters obtained with the k-means clustering are shown in Figure 5. For each frequency band, the clusters reflected the reorganization obtained previously (Figures 3 and 4). Cluster 1 corresponded to the ROIs with positive difference in NE/CC in patients versus controls; cluster 3 regrouped the ROIs with negative difference in NE/CC in patients versus controls; cluster 2 combined the ROIs with similar NE/CC in patients versus controls. The following results will refer to the *t*-tests comparing the meta-connectivity of patients and controls. The

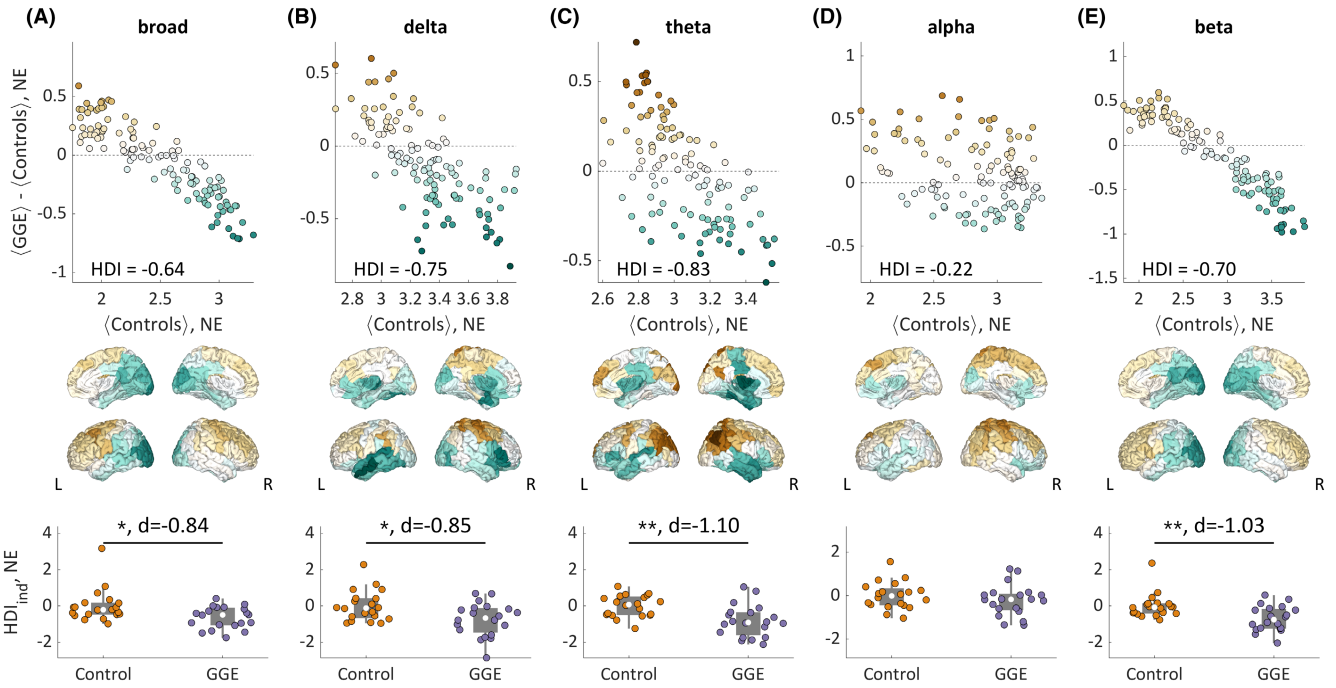

FIGURE 3 Hub Disruption Index (HDI) of the nodal efficiency (NE) across frequency bands (A: broad, B: delta, C: theta, D: alpha, E: beta). In the top panels, the difference of the average NE between groups (⟨GGE⟩-⟨Controls⟩, y-axis) is plotted against the average value of NE in the healthy control group (⟨Controls⟩, x-axis). Each data point is color-coded according to the value of the difference in NE between groups and represents one region of interest (ROI). The slope of the scatterplot gives the global HDI for the genetic generalized epilepsy (GGE) group. Negative HDI indicates disruption of NE; ROIs with high values in controls have lower values in patients (dark green), and ROIs with low values in controls have higher values in patients (dark brown). The middle panels represent the topography of the reorganization. The ROIs are color-coded as in the above scatterplot, that is, according to the value of the difference in NE between groups. ROIs colored dark green are important in transferring information in the network of controls but less so in that of patients. Similarly, ROIs colored dark brown play a crucial role in patients but are the least important in controls. In the bottom panels, the swarm plots and boxplots represent the values of the individual HDI calculated for each participant or patient. The individual HDIs are obtained by using the ROI network features of each participant individually, instead of the average across the GGE group as in the global HDI. A two-sided two-sample *t*-test assessed the difference between groups (*$p < .05$, **$p < .01$, false discovery rate corrected for 10 comparisons). Cohen's *d* gives the effect size of the test. GGE, Genetic generalized epilepsy; HDI, Hub Disruption Index; NE, nodal efficiency; ROI, region of interest; ⟨.⟩, group average. L, left; R, right.

obtained results were similar in the delta, theta, and beta frequency bands. Cluster 1 had higher within connectivity (δ: $p = .0022$, θ: $p < .001$, β: $p = .038$) and cluster 3 had lower within connectivity (δ: $p = .014$, θ: $p = .017$, β: $p = .017$) in patients than in controls. Cluster 2 was more connected to cluster 1 (δ: $p = .014$, θ: $p = .0013$, β: $p = .014$) and less connected to cluster 3 (δ: $p = .035$, θ: $p = .0013$, β: $p = .020$). In summary, in patients, the increase in NE/CC in cluster 1's ROIs came with an increase in within connectivity and connectivity to cluster 2's ROIs, whereas the decrease in NE/CC in cluster 3's ROIs was accompanied by a decrease in within connectivity and connectivity to cluster 2's ROIs.

3.5 | HDI and clinical variables

The individual HDI was not significantly correlated ($p > .05$, uncorrected) with the age at epilepsy onset or epilepsy duration in any frequency bands or network measures. We also did not find any significant correlation ($p > .05$, uncorrected) between individual HDI and drug load or spike rate. The results of the correlation are given in Table S2.

3.6 | HDI with low-density EEG

After reducing the hdEEG montage to a standard EEG montage, and recomputing the HDI for previously significant frequency bands, we obtained similar results to those obtained with hdEEG (Figure 6). The topographies of the reorganization of NE and CC were similar to the previous ones, significant in delta and theta frequency bands, and the effect size were still large (broad: $t = -1.58|-1.23$, $p = .14|.22$, $d = -.50|-.39$; δ: $t = -4.32|-3.96$, $p < .001$, $d = -1.36|-1.25$; θ: $t = -4.11|-4.10$, $p < .001$, $d = -1.30|-1.29$; β: $t = -2.17|-1.88$, $p = .059|.09$, $d = -.68|-.60$).

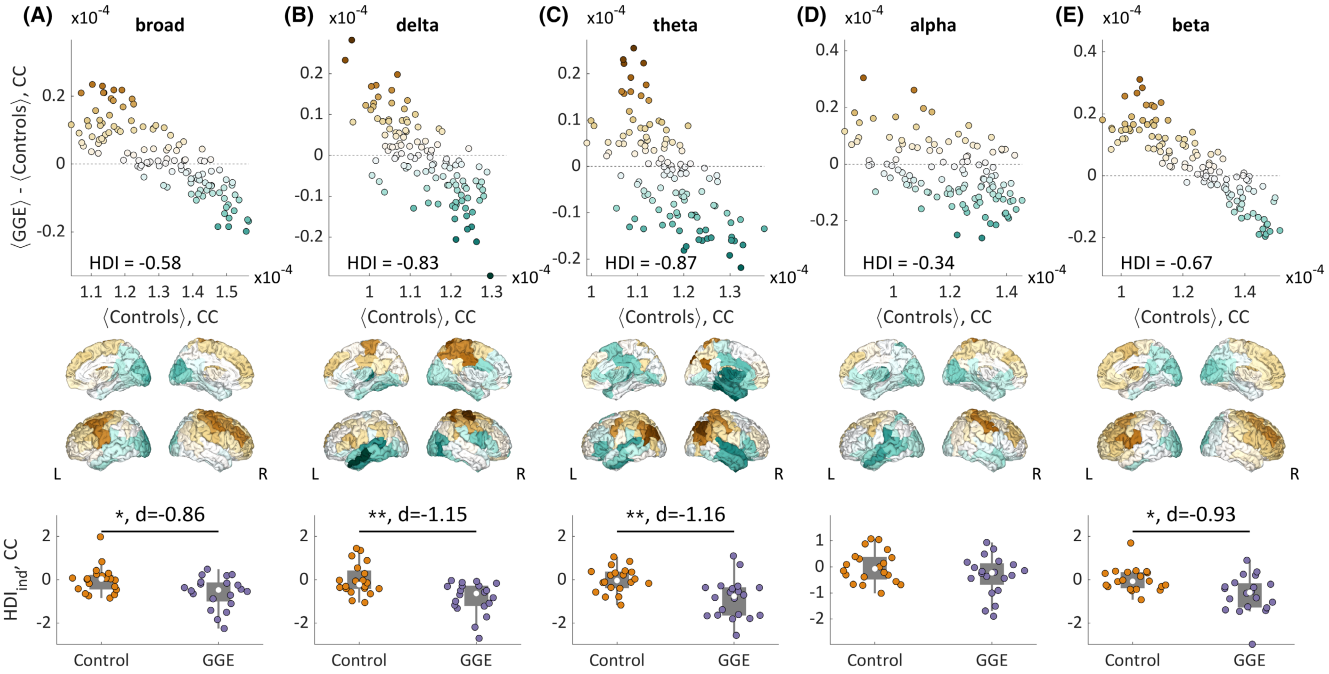

FIGURE 4 Hub Disruption Index (HDI) of the clustering coefficient (CC) across frequency bands (A: broad, B: delta, C: theta, D: alpha, E: beta). The organization of this figure follows that of Figure 3. The top panels show the scatterplot to compute the group HDI for the clustering coefficient, the middle panels illustrate the topography of the disruptions, and the bottom panels display the individual HDIs with the result of the statistical tests (*$p < .05$, **$p < .01$, false discovery rate corrected for 10 comparisons) and their effect size. GGE, genetic generalized epilepsy; L, left; R, right, ⟨.⟩, group average.

4 | DISCUSSION

In the present study, we investigated whether patients with GGE and sex- and age-matched healthy controls can be differentiated using global and local properties of the whole-brain functional network derived from interictal hdEEG. We report that patients with GGE and healthy controls have similar global network integration and segregation. However, the local properties were strongly reorganized in a space- and frequency-dependent fashion. In other words, global brain network topological properties were preserved under pathological conditions, whereas the importance of specific regions in distributing neural information across the network had been interchanged, which can be viewed as a form of homeostasis. With to the meta-connectivity analysis, we showed that the connectivity within the same groups of regions mirrored the local change in integration and segregation. Finally, we reproduced these findings using a clinical 25-electrode EEG setting.

4.1 | Homeostatically preserved brain network topology

Homeostasis is a process by which living systems tend to maintain the equilibrium of internal conditions (e.g., body temperature). Our results suggest that the human brain tends to balance whole-brain integration and segregation in such a way under healthy or pathological conditions. In line with our results, a recent review and a meta-analysis reported that most of the studies comparing brain global network topology between patients with GGE and healthy controls in EEG/MEG showed no differences.[14,15] We went further and showed that the local integration and segregation are higher in some regions and lower in others, both effects balancing each other at the whole-brain level. This alteration of network topology occurs mainly within areas whose inner functional connectivity is increased or decreased, respectively. This homeostasislike behavior in network properties has been found in other neurological conditions (e.g., disorders of consciousness,[16] neuromyelitis optica spectrum disorder,[37] and stroke[38]) and has been shown to be a robust estimator of brain network reorganization.[38]

A common misconception in GGE is to consider the involvement of the whole brain homogeneously. In actuality, GSW show typically a bifrontal preponderance in EEG,[1] and generalized spike wave discharges have been shown to trigger activation in regions of the DMN at seizure onset in fMRI studies.[5,39] Our finding of local increase in integration, segregation, and connectivity strength found in the prefrontal cortex in the beta band and in the regions of the DMN in the theta band is in agreement with the above statements and points toward epileptic networks distributed with a clear spatial and spectral specificity in GGE.

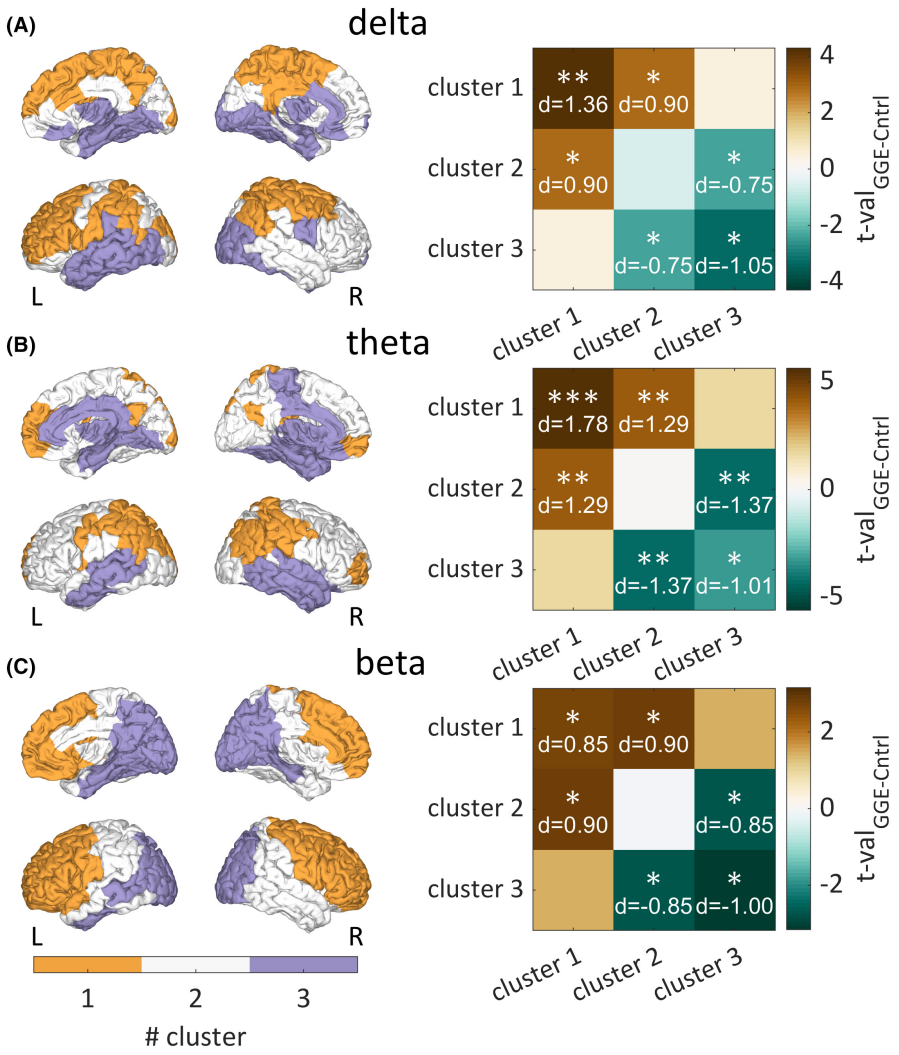

FIGURE 5 Meta-connectivity analysis across the three significant narrow frequency bands (A: delta, B: theta, C: beta), genetic generalized epilepsy (GGE) versus controls. The three clusters obtained using a k-means algorithm on the four variables of the scatterplots of Figures 3 and 4 are represented on brain meshes for three significant narrow frequency bands. Cluster 1 (orange) represents the regions of interest (ROIs) where the difference in nodal efficiency (NE) and clustering coefficient (CC) were positive (brown ROIs in Figures 3 and 4), cluster 3 (purple) regroups the ROIs where the difference in NE and CC were negative (green ROIs in Figures 3 and 4), and cluster 2 (white) brings together ROIs that have similar levels of NE and CC in both groups (white ROIs in Figures 3 and 4). The meta-connectivity matrix is obtained by averaging the connectivity values of each ROI belonging to the investigated clusters, yielding a symmetric 3-by-3 meta-connectivity matrix (detailed in Figure 1). A two-sided two-sample *t*-test assessed the difference in meta-connectivity between groups (*$p < .05$, **$p < .01$, ***$p < .001$, false discovery rate corrected for 18 comparisons). Cohen's *d* gives the effect size of the test. CC, Clustering coefficient; Cntrl, control; L, left; R, right.

No change was found in the alpha band, possibly because the visual network, whose activity is predominant in this frequency band, was unaffected. Increased segregation and integration respectively suggest that regions of these networks are more densely interconnected and that the communication between any two regions, even distant, is more efficient. This could possibly promote the spread of pathological activities within these regions. However, we also showed that other areas exhibited a reduction in those features. This reorganization could be a coping mechanism to limit the spread of these pathological activities, while maintaining an overall efficient network. Disruption of this homeostasis could possibly lead to seizure, as modifications in the activity and connectivity of the DMN is observed during absence seizures.[5,40] Mechanisms promoting and disrupting this homeostasis remain an open question for further investigations.

4.2 | Network reconfiguration and cognitive deficits

Patients with GGE generally suffer from impairment of executive functions, which is a heavy burden on daily

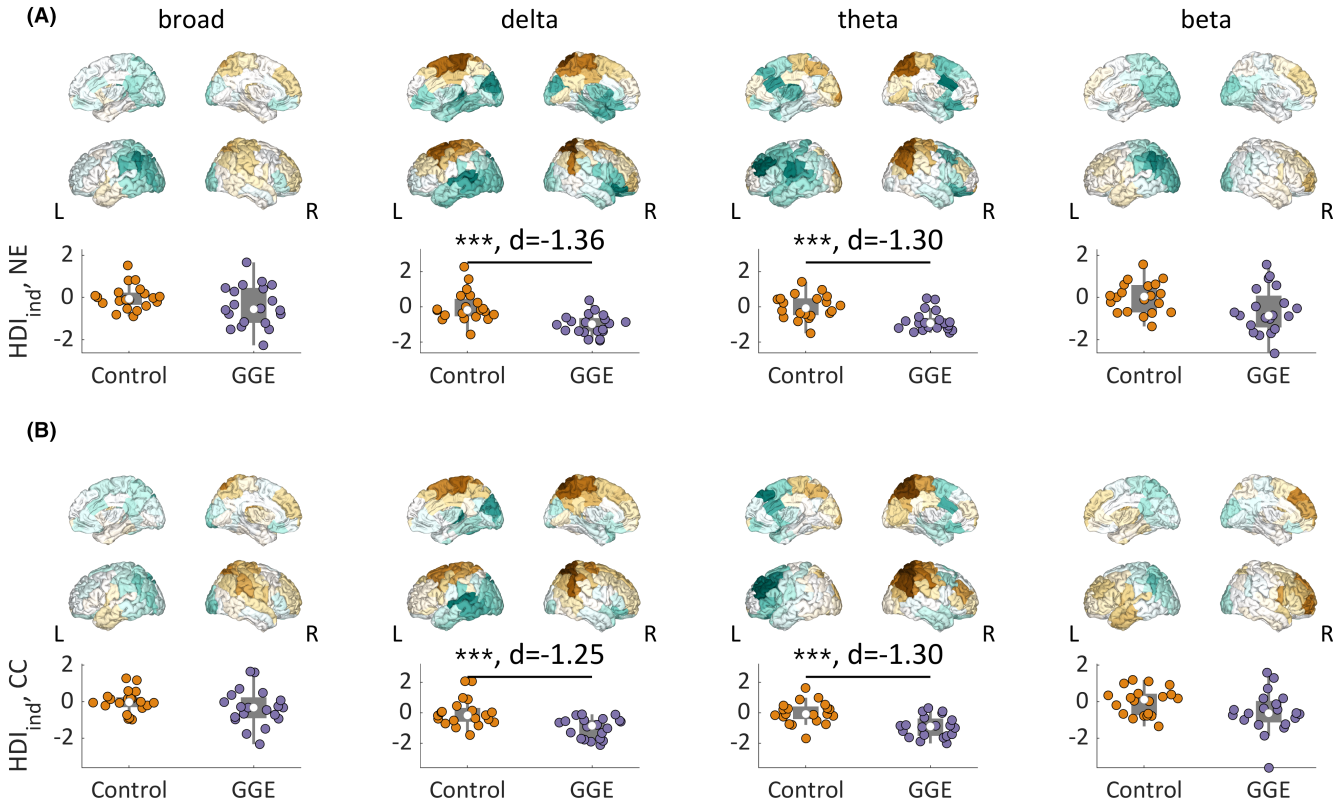

FIGURE 6 Standard (low-density) electroencephalographic (EEG) Hub Disruption Index (HDI) of nodal efficiency (NE) and clustering coefficient (CC) across the different frequency bands, which were significant in the high-density EEG (hdEEG) analysis. The topography of the disruption is given in the top panels and the individual HDIs are shown in the bottom panel as swarm plots and boxplots across frequency bands, concordant with the hdEEG, for NE (A) and CC (B). The individual HDIs are significant for the delta and theta frequency bands (***$p < .001$, false discovery rate corrected for eight comparisons). GGE, genetic generalized epilepsy; L, left; R, right.

life.[41] In the theta band, we showed that ROIs from the DMN were more influential in patients, whereas those of the salience network (SN), limbic system, and temporal network were less. The interplay of the DMN with the executive and attentional networks is critical for successful cognitive processes.[6] The preponderance of the DMN over the SN, in terms of both integration/segregation and connectivity, may have a role in these cognitive impairments. Furthermore, we showed a clear split between the frontal and the posterior areas in the beta band. Beta oscillations are generally associated with local processing. Such a difference between frontal and posterior regions—which both support executive functions—could also play an important role in executive function impairment in GGE.

4.3 | HDI as diagnostic tool specific to GGE

Diagnosis of GGE is made in 80% of patients after examination of clinical history and a single routine EEG.[2] For the remaining 20% of patients, additional investigations are required. The large effect size of the HDI suggests that GGE and healthy controls are well separable even in the absence of IEDs. Moreover, we reproduced our findings with standard 25-channel EEG, again with large effect sizes. This measure could thus potentially be used as an additional routine clinical tool, without the need for hdEEG and visible IEDs. Applying source reconstruction to EEG recorded with <64 channels[42] reduces spatial resolution and localization accuracy in presurgical evaluations. In our case, the disruption occurred in large cortical areas, indicating that fine spatial resolution was not a critical point. Validation of our results on a larger dataset, possibly including a drug-naive cohort, is however required. For clinical application, it is also crucial to distinguish GGE from focal epilepsy, which can be difficult in some instances. Few studies have investigated the HDI in focal epilepsy and, to the best of our knowledge, only using fMRI. A disruption in integration and segregation was found in patients with right, but not left, temporal lobe epilepsy.[43] Another study found an asymmetrical disruption in patients with temporal lobe epilepsy within mesial temporal lobe and the DMN, but the HDI was not studied at the whole-brain level.[44] A disruption was also found in a sample

group of patients with various types of focal epilepsy.[45] The topography of the disruption did not match any fMRI network, unlike our results in GGE, and was accompanied by a difference in local and global efficiencies of the whole-brain network. Moreover, previous studies from our group have reported an increase in GE in patients with temporal epilepsy and more specifically in the ipsilateral hemisphere using hdEEG.[11,46] First, such an increase goes against the definition of the HDI and suggests absence of preserved topology. Second, even if such EEG-based disruption occurs in focal epilepsy patients, the topographies are expected to differ from those in GGE and align with the location of the epileptogenic zone, distorting the point cloud nonlinearly and violating the HDI principle. The disruption found in GGE was, however, symmetrical and engaged both hemispheres. We hypothesize that the HDI of GGE patients in its spatiofrequential content is specific to GGE and should be absent in patients with focal epilepsy.

4.4 | Methodological considerations

There are limitations to our study. First, we aggregated data from patients diagnosed with different GGE syndromes due to small subgroup sample size. These syndromes, however, share similar genetic background, EEG manifestations, and semiology (see Vorderwülbecke et al.[2] for review). Core networks are expected to be common to these syndromes. Under the opposite hypothesis, the reorganization topography should have been syndrome dependent. As the order of the ROIs on the x-axis is fixed by the control group and the effect size was large, it seems unlikely that such a syndrome-dependent reorganization is preponderant in the studied frequency bands.

Second, it is not possible to rule out drug treatment as a confounding factor. The ASM effect recognized on visual EEG analysis consists of increased beta activity with a frontal predominance, mostly for benzodiazepine but also some other drugs (e.g., lamotrigine).[47] Two patients were treated with benzodiazepine and six with lamotrigine. We found increased NE and CC in the anterior regions in the beta frequency band, but also reduced NE and CC in posterior regions. These drugs also have different mechanism of actions and the individual HDI was not correlated to the drug load, supporting a potential minor effect of the treatment. For practical reasons, hdEEG recording in drug-naive patients is difficult, usually due to treatment initiation in the emergency room admission or shortly afterward, preventing the opportunity to organize hdEEG.

Future investigations should therefore investigate a larger cohort and eventually investigate this network reorganization in drug-naive patients with suspected GGE and focal epilepsy using standard EEG obtained routinely before treatment initiation. We showed that this network reorganization can be captured at low density, and routine low-density EEG is generally the only available EEG recording at that stage of the diagnosis.

AUTHOR CONTRIBUTIONS

André Silva Alves: Conceptualization; data acquisition & curation; methodology; formal analysis; writing–original draft; writing–review & editing. **Isotta Rigoni:** Data acquisition & curation; methodology; writing–review & editing. **Pierre Mégevand:** Methodology; writing–review & editing. **Stanislas Lagarde:** Data curation; methodology; writing–review & editing. **Fabienne Picard:** Methodology; writing–review & editing. **Margitta Seeck:** Methodology; writing–review & editing. **Serge Vulliémoz:** Conceptualization; supervision; funding acquisition; writing–review & editing. **Nicolas Roehri:** Conceptualization; methodology; data acquisition & curation; formal analysis; supervision; writing–review & editing.

ACKNOWLEDGMENTS

This work was supported by Swiss National Science Foundation (SNSF) grants 192749, 170873, and 209470 to S.V. and 180365 to M.S. P.M. was funded by SNSF Career Award 194507. N.R. was supported by the SNSF Ambizione grant 209120. S.L. was supported by the LFCE (Ligue Française Contre l'Epilepsie, French chapter of the International League Against Epilepsy) and PHOCEO (fonds de dotation de l'AP-HM). Open access funding provided by Universite de Geneve.

CONFLICT OF INTEREST STATEMENT

M.S. and S.V. have shares in Epilog. The other authors report no competing interests.

DATA AVAILABILITY STATEMENT

The raw data that support the findings of this study are available on reasonable request from the corresponding author. The raw data are not publicly available, as they could containing information that could compromise the privacy of research participants. Derived data (e.g., connectivity matrices, derived network measures (NE, GE, CC, ⟨CC⟩, and HDI) for each frequency band) as well as the results of the statistical tests are available here: https://doi.org/10.6084/m9.figshare.23702514.v1

ETHICS STATEMENT

The study was approved by the Geneva ethical committee (protocol #2020-02526). This research project was conducted in accordance with Swiss regulations and with the Declaration of Helsinki. Healthy controls and patients

have signed a consent form. We confirm that we have read the Journal's position on issues involved in ethical publication and affirm that this report is consistent with those guidelines.

ORCID

André Silva Alves https://orcid.org/0000-0002-4088-5048
Isotta Rigoni https://orcid.org/0000-0002-5804-2137
Pierre Mégevand https://orcid.org/0000-0002-0427-547X
Stanislas Lagarde https://orcid.org/0000-0003-2916-1302
Fabienne Picard https://orcid.org/0000-0001-9120-1761
Margitta Seeck https://orcid.org/0000-0002-6702-0167
Serge Vulliémoz https://orcid.org/0000-0002-1877-8625
Nicolas Roehri https://orcid.org/0000-0002-6948-1055

REFERENCES

1. Hirsch E, French J, Scheffer IE, Bogacz A, Alsaadi T, Sperling MR, et al. ILAE definition of the idiopathic generalized epilepsy syndromes: position statement by the ILAE Task Force on Nosology and Definitions. Epilepsia. 2022;63(6):1475–99.
2. Vorderwülbecke BJ, Wandschneider B, Weber Y, Holtkamp M. Genetic generalized epilepsies in adults — challenging assumptions and dogmas. Nat Rev Neurol. 2022;18(2):71–83.
3. Sakurai K, Takeda Y, Tanaka N, Kurita T, Shiraishi H, Takeuchi F, et al. Generalized spike-wave discharges involve a default mode network in patients with juvenile absence epilepsy: a MEG study. Epilepsy Res. 2010;89(2–3):176–84. https://doi.org/10.1016/j.eplepsyres.2009.12.004
4. Aghakhani Y, Bagshaw AP, Bénar CG, Hawco C, Andermann F, Dubeau F, et al. fMRI activation during spike and wave discharges in idiopathic generalized epilepsy. Brain. 2004;127(5):1127–44.
5. Tangwiriyasakul C, Perani S, Centeno M, Yaakub SN, Abela E, Carmichael DW, et al. Dynamic brain network states in human generalized spike-wave discharges. Brain. 2018;141(10):2981–94.
6. Raichle ME. The brain's default mode network. Annu Rev Neurosci. 2015;38:433–47.
7. Focke NK, Diederich C, Helms G, Nitsche MA, Lerche H, Paulus W. Idiopathic-generalized epilepsy shows profound white matter diffusion-tensor imaging alterations. Hum Brain Mapp. 2014;35:3332–42.
8. Bin G, Wang T, Zeng H, He X, Li F, Zhang J, et al. Patterns of gray matter abnormalities in idiopathic generalized epilepsy: a meta-analysis of voxel-based morphology studies. PLoS One. 2017;12(1):1–11.
9. Mckavanagh A, Kreilkamp BAK, Chen Y, Denby C, Bracewell M, Das K, et al. Altered structural brain networks in refractory and nonrefractory idiopathic generalized epilepsy. Brain Connect. 2022;12(6):549–60.
10. Lagarde S, Roehri N, Lambert I, Trebuchon A, McGonigal A, Carron R, et al. Interictal stereotactic-EEG functional connectivity in refractory focal epilepsies. Brain. 2018;141(10):2966–80.
11. Coito A, Biethahn S, Tepperberg J, Carboni M, Roelcke U, Seeck M, et al. Interictal epileptogenic zone localization in patients with focal epilepsy using electric source imaging and directed functional connectivity from low-density EEG. Epilepsia Open. 2019;4(2):281–92.
12. Narasimhan S, Kundassery KB, Gupta K, Johnson GW, Wills KE, Goodale SE, et al. Seizure-onset regions demonstrate high inward directed connectivity during resting-state: an SEEG study in focal epilepsy. Epilepsia. 2020;61(11):2534–44. https://doi.org/10.1111/epi.16686
13. Elshahabi A, Klamer S, Sahib AK, Lerche H, Braun C, Focke NK. Magnetoencephalography reveals a widespread increase in network connectivity in idiopathic/genetic generalized epilepsy. PLoS One. 2015;10(9):1–16.
14. Pegg EJ, Taylor JR, Keller SS, Mohanraj R. Interictal structural and functional connectivity in idiopathic generalized epilepsy: a systematic review of graph theoretical studies. Epilepsy Behav. 2020;106:107013. https://doi.org/10.1016/j.yebeh.2020.107013
15. Dharan AL, Bowden SC, Lai A, Peterson ADH, Cheung MWL, Woldman W, et al. Resting-state functional connectivity in the idiopathic generalized epilepsies: a systematic review and meta-analysis of EEG and MEG studies. Epilepsy Behav. 2021;124:108336. https://doi.org/10.1016/j.yebeh.2021.108336
16. Achard S, Delon-Martin C, Vértes PE, Renard F, Schenck M, Schneider F, et al. Hubs of brain functional networks are radically reorganized in comatose patients. Proc Natl Acad Sci USA. 2012;109(50):20608–13.
17. Jung TP, Makeig S, Humphries C, Lee TW, McKeown MJ, Iragui V, et al. Removing electroencephalographic artifacts by blind source separation. Psychophysiology. 2000;37(2):163–78.
18. Perrin F, Pernier J, Bertrand O, Echallier JF. Spherical splines for scalp potential and current density mapping. Electroencephalogr Clin Neurophysiol. 1989;72(2):184–7.
19. Vorderwülbecke BJ, Carboni M, Tourbier S, Brunet D, Seeber M, Spinelli L, et al. High-density electric source imaging of interictal epileptic discharges: how many electrodes and which time point? Clin Neurophysiol. 2020;131(12):2795–803.
20. Oostenveld R, Fries P, Maris E, Schoffelen JM. FieldTrip: open source software for advanced analysis of MEG, EEG, and invasive electrophysiological data. Comput Intell Neurosci. 2011;2011:1–9.
21. Hagmann P, Cammoun L, Gigandet X, Meuli R, Honey CJ, Wedeen VJ, et al. Mapping the structural core of human cerebral cortex. PLoS Biol. 2008;6(7):1479–93.
22. Cammoun L, Gigandet X, Meskaldji D, Thiran JP, Sporns O, Do KQ, et al. Mapping the human connectome at multiple scales with diffusion spectrum MRI. J Neurosci Methods. 2012;203(2):386–97. https://doi.org/10.1016/j.jneumeth.2011.09.031
23. FreeSurfer FB. FreeSurfer. Neuroimage. 2012;62(2):774–81.
24. Tourbier S, Aleman-Gomez Y, Griffa A, Bach Cuadra M, Hagmann P. Connectome mapper v3.0.0-beta-20200206. 2020.
25. Tourbier S, Rue-Queralt J, Glomb K, Aleman-Gomez Y, Mullier E, Griffa A, et al. Connectome mapper 3: a flexible and open-source pipeline software for multiscale multimodal human connectome mapping. J Open Source Softw. 2022;7(74):4248.
26. Gramfort A, Papadopoulo T, Olivi E, Clerc M. OpenMEEG: opensource software for quasistatic bioelectromagnetics. Biomed Eng Online. 2010;9(1):45. https://doi.org/10.1186/1475-925X-8-1

27. Pascual-Marqui RD. Discrete, 3D distributed, linear imaging methods of electric neuronal activity. Part 1: exact, zero error localization. *arXiv*. 2007;1–16. https://doi.org/10.48550/arXiv.0710.3341
28. Rubega M, Carboni M, Seeber M, Pascucci D, Tourbier S, Toscano G, et al. Estimating EEG source dipole orientation based on singular-value decomposition for connectivity analysis. Brain Topogr. 2019;32(4):704–19. https://doi.org/10.1007/s10548-018-0691-2
29. Vinck M, Oostenveld R, van Wingerden M, Battaglia F, Pennartz CM. An improved index of phase-synchronization for electrophysiological data in the presence of volume-conduction, noise and sample-size bias. Neuroimage. 2011;55(4):1548–65. https://doi.org/10.1016/j.neuroimage.2011.01.055
30. Rubinov M, Sporns O. Complex network measures of brain connectivity: uses and interpretations. Neuroimage. 2010;52(3):1059–69. https://doi.org/10.1016/j.neuroimage.2009.10.003
31. Latora V, Marchiori M. Efficient behavior of small-world networks. Phys Rev Lett. 2001;87(19):198701.
32. Onnela JP, Saramäki J, Kertész J, Kaski K. Intensity and coherence of motifs in weighted complex networks. Phys Rev E Stat Nonlin Soft Matter Phys. 2005;71(6):065103.
33. Watts DJ, Strogatz SH. Collective dynamics of 'small-world' networks. Nature. 1998;393:440–2.
34. Witt JA, Nass RD, Baumgartner T, von Wrede R, Elger CE, Surges R, et al. Does the accumulated antiepileptic drug load in chronic epilepsy reflect disease severity? Epilepsia. 2020;61(12):2685–95.
35. Seeck M, Koessler L, Bast T, Leijten F, Michel C, Baumgartner C, et al. The standardized EEG electrode array of the IFCN. Clin Neurophysiol. 2017;128(10):2070–7. https://doi.org/10.1016/j.clinph.2017.06.254
36. Benjamini Y, Hochberg Y. Controlling the false discovery rate: a practical and powerful approach to multiple testing. J R Stat Soc Ser B Methodol. 1995;57(1):289–300.
37. Bigaut K, Achard S, Hemmert C, Baloglu S, Kremer L, Collongues N, et al. Resting-state functional MRI demonstrates brain network reorganization in neuromyelitis optica spectrum disorder (NMOSD). PLoS One. 2019;14(1):1–10.
38. Termenon M, Achard S, Jaillard A, Delon-Martin C. The "hub disruption index," a reliable index sensitive to the brain networks reorganization. A study of the Contralesional hemisphere in stroke. Front Comput Neurosci. 2016;10:1–15.
39. Bai X, Vestal M, Berman R, Negishi M, Spann M, Vega C, et al. Dynamic time course of typical childhood absence seizures: EEG, behavior, and functional magnetic resonance imaging. J Neurosci. 2010;30(17):5884–93.
40. Guo JN, Kim R, Chen Y, Negishi M, Jhun S, Weiss S, et al. Impaired consciousness in patients with absence seizures investigated by functional MRI, EEG, and behavioural measures: a cross-sectional study. Lancet Neurol. 2016;15(13):1336–45. https://doi.org/10.1016/S1474-4422(16)30295-2
41. Ratcliffe C, Wandschneider B, Baxendale S, Thompson P, Koepp MJ, Caciagli L. Cognitive function in genetic generalized epilepsies: insights from neuropsychology and neuroimaging. Front Neurol. 2020;11:144.
42. Michel CM, Brunet D. EEG source imaging: a practical review of the analysis steps. Front Neurol. 2019;10:325.
43. Ridley BGY, Rousseau C, Wirsich J, le Troter A, Soulier E, Confort-Gouny S, et al. Nodal approach reveals differential impact of lateralized focal epilepsies on hub reorganization. Neuroimage. 2015;118:39–48. https://doi.org/10.1016/j.neuroimage.2015.05.096
44. Lee K, Khoo HM, Lina JM, Dubeau F, Gotman J, Grova C. Disruption, emergence and lateralization of brain network hubs in mesial temporal lobe epilepsy. Neuroimage Clin. 2018;20:71–84. https://doi.org/10.1016/j.nicl.2018.06.029
45. Song J, Nair VA, Gaggl W, Prabhakaran V. Disrupted brain functional organization in epilepsy revealed by graph theory analysis. Brain Connect. 2015;5(5):276–83.
46. Carboni M, Rubega M, Iannotti GR, de Stefano P, Toscano G, Tourbier S, et al. The network integration of epileptic activity in relation to surgical outcome. Clin Neurophysiol. 2019;130(12):2193–202. https://doi.org/10.1016/j.clinph.2019.09.006
47. Kozelka JW, Pedley TA. Beta and mu rhythms. J Clin Neurophysiol. 1990;7(2):191–207.

SUPPORTING INFORMATION

Additional supporting information can be found online in the Supporting Information section at the end of this article.

How to cite this article: Silva Alves A, Rigoni I, Mégevand P, Lagarde S, Picard F, Seeck M, et al. High-density electroencephalographic functional networks in genetic generalized epilepsy: Preserved whole-brain topology hides local reorganization. Epilepsia. 2024;65:961–973. https://doi.org/10.1111/epi.17903